A multifunctional shape-morphing elastomer with liquid metal inclusions

Michael J. Ford[a], Cedric P. Ambulo[b], Teresa A. Kent[a], Eric J. Markvicka[c,d], Chengfeng Pan[a], Jonathan Malen[a], Taylor H. Ware[b], and Carmel Majidi[a,c,e,1]

[a]Department of Mechanical Engineering, Carnegie Mellon University, Pittsburgh, PA 15213; [b]Department of Bioengineering, University of Texas at Dallas, Richardson, TX 75080; [c]Robotics Institute, Carnegie Mellon University, Pittsburgh, PA 15213; [d]Department of Mechanical and Materials Engineering, University of Nebraska–Lincoln, Lincoln, NE 68588; and [e]Department of Materials Science and Engineering, Carnegie Mellon University, Pittsburgh, PA 15213

Edited by John A. Rogers, Northwestern University, Evanston, IL, and approved September 13, 2019 (received for review June 26, 2019)

Natural soft tissue achieves a rich variety of functionality through a hierarchy of molecular, microscale, and mesoscale structures and ordering. Inspired by such architectures, we introduce a soft, multifunctional composite capable of a unique combination of sensing, mechanically robust electronic connectivity, and active shape morphing. The material is composed of a compliant and deformable liquid crystal elastomer (LCE) matrix that can achieve macroscopic shape change through a liquid crystal phase transition. The matrix is dispersed with liquid metal (LM) microparticles that are used to tailor the thermal and electrical conductivity of the LCE without detrimentally altering its mechanical or shape-morphing properties. Demonstrations of this composite for sensing, actuation, circuitry, and soft robot locomotion suggest the potential for versatile, tissue-like multifunctionality.

liquid crystal elastomer | liquid metal | shape memory | conductive elastomer | soft actuator

Condensed soft matter such as elastomers, gels, and fluids have emerged as functional building blocks for soft machines and electronics (1–3). Such efforts have yielded breakthrough material architectures that are mechanically compliant, deformable, and capable of some combination of sensing, signal transmission, shape morphing, or autonomously self-reconfiguring capabilities, thereby emulating the rich multifunctionality observed in biological skin, muscle, and nervous tissue (4–7). Among state-of-the-art soft multifunctional materials, liquid crystal elastomers (LCEs) are especially promising since LCEs exhibit the largest thermally induced reversible deformation of any solid material (1). Notably, LCEs contract on heating and expand on cooling with thermoreversible strains of up to 400% (8). However, ambient heating is often used to drive shape change, and this approach fundamentally limits the speed, efficiency, and utility of LCEs in practical applications.

Previously, rigid nanoparticles have been used as surface heating elements or as fillers for LCE and related composites that are electrically responsive, magnetically responsive, and/or photoresponsive (9–13). However, surface heating elements are limited in applicability beyond thicknesses of a few hundred micrometers due to the low intrinsic thermal conductivity of LCEs (14). Furthermore, rigid components alter the mechanical properties and constrain the shape-changing capabilities of the surrounding LCE. For example, Agrawal et al. showed that the electrical resistance was too high for Joule-heated actuation of a bulk carbon black–LCE composite until 15 wt % carbon black was added. At 15 wt % carbon black, the actuation strain reduced from 35.0% in the unfilled LCE to 5.2% in the filled LCE, necessitating surface heating (15). With that in mind, LCE composites are often synthesized with a low weight content (i.e., less than a few percent) of filler particles, which significantly restricts the allowable thermal and electrical conductivity and necessitates the addition of surface heaters/devices for actuation and sensing (16). In addition to heating, actuation can also be achieved through a photochemical transition, in which light absorption reduces molecular order through the isomerization of a dye such as azobenzene and drives macroscopic shape change. However, such responses are only possible in relatively thin films due to the strong absorption of azobenzene and thus limit diversity in form factors. Overall, the limitations of the methods used to trigger shape change in LCEs have restricted broader applications of these materials. Furthermore, design of multifunctional LCE composites has been further limited by the detrimental effects of functional fillers (e.g., rigidity that inhibits deformability and/or LC phase transition) (15) on shape-change capabilities.

Here, we overcome the aforementioned limitations by introducing a material architecture that dramatically expands the range of properties and dynamic functionalities that can be achieved with LCEs. Multifunctionality is accomplished by embedding the LCE with liquid metal (LM) microdroplets (Fig. 1 *A*–*C*). Because the inclusions are liquid at room temperature, they are able to freely deform with the surrounding matrix when the composite is stretched (Fig. 1 *D* and *E*). Moreover, the LM inclusions do not interfere with the ability of the LCE to change shape and perform mechanical work in response to external stimuli (Fig. 1*F*). Shape morphing in the absence of an external load can be programmed into the LCE–LM composite through photoinitiated cross-linking so that it can reversibly transition between preprogrammed morphologies through electrical or thermal

Significance

Research in soft robotics and wearable technologies has led to increasing demand for shape-changing materials that can be powered with portable electronics. Liquid crystal elastomers (LCEs) are a promising functional material for these applications but lack the electrical and thermal conductivity required for electrically stimulated shape-memory activation. To address this, LCEs are typically embedded with rigid fillers that enhance conductivity. However, these particles degrade the mechanical properties and shape-morphing capabilities of the LCE matrix. Here, we overcome these limitations with an advanced material architecture in which rigid filler is replaced with deformable liquid metal inclusions. This results in LCE composites that exhibit a combination of high electrical conductivity, high thermal conductivity, and actuation capabilities unlike any other soft composite.

Author contributions: M.J.F., C.P.A., T.A.K., E.J.M., C.P., J.M., T.H.W., and C.M. designed research; M.J.F., C.P.A., T.A.K., E.J.M., and C.P. performed research; M.J.F., C.P.A., J.M., T.H.W., and C.M. analyzed data; and M.J.F., C.P.A., J.M., T.H.W., and C.M. wrote the paper.

The authors declare no competing interest.

This article is a PNAS Direct Submission.

[1]To whom correspondence may be addressed. Email: cmajidi@andrew.cmu.edu.

This article contains supporting information online at www.pnas.org/lookup/suppl/doi:10.1073/pnas.1911021116/-/DCSupplemental.

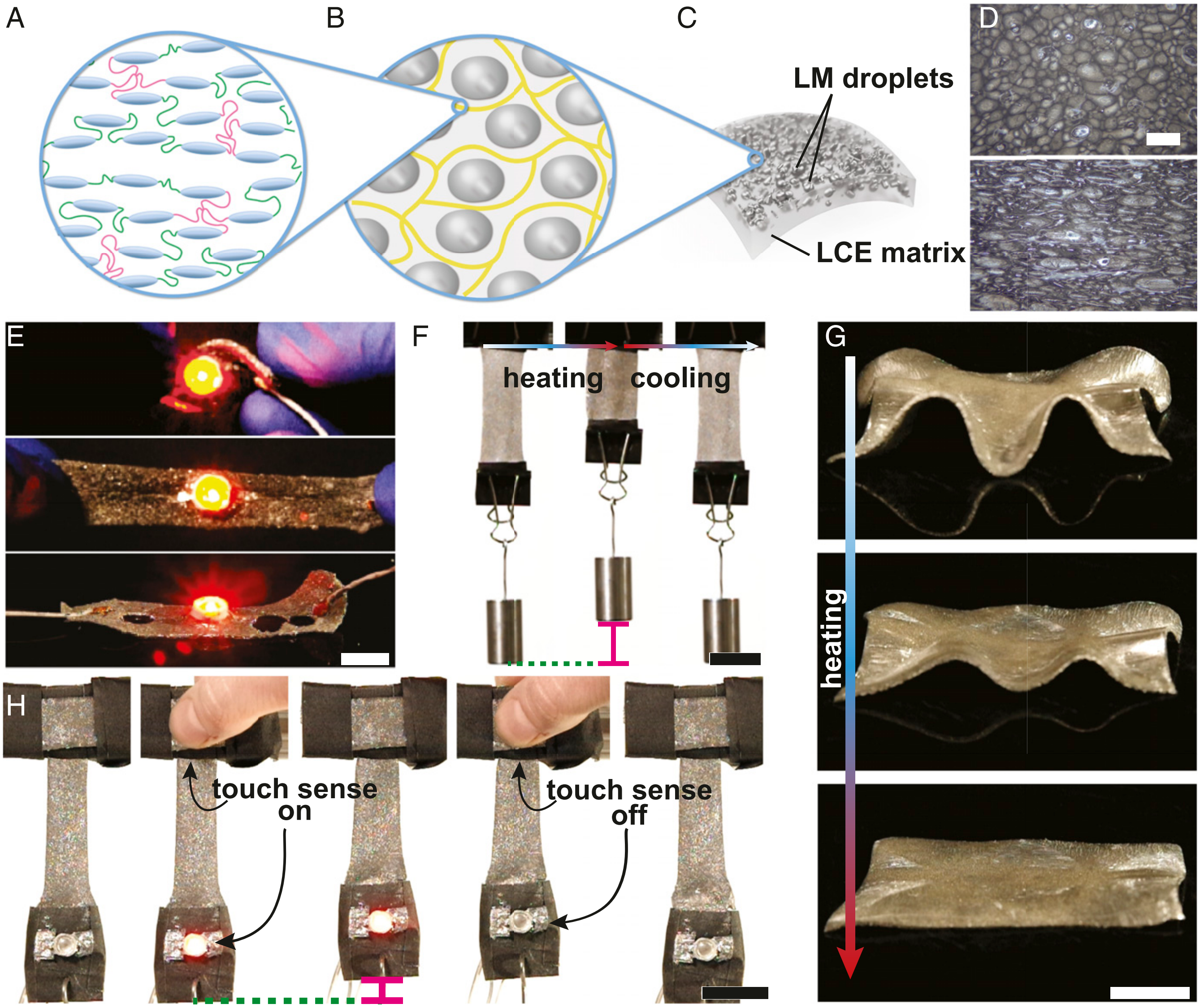

Fig. 1. LM–LCE composites and related functional demonstrations. Illustrations of the molecular (*A*), microscale (*B*), and mesoscale (*C*) ordering of LM–LCE composites. (*D*) Micrographs of unstrained (*Top*) and strained (*Bottom*) composites. (Scale bars, 1 mm.) (*E*) Photographs highlighting the compliance and deformability of an unstretched (*Top*) and stretched (*Middle*) electrically conductive 50 vol % LM–LCE powering an LED. Circuit traces form through mechanical damage (*Bottom*). (Scale bar, 1 cm.) (*F*) Photographs of a 50 vol % LM–LCE composite lifting a 100-g weight (~45 kPa). (Scale bar, 3 cm.) (*G*) Photographs of zero-stress shape change enabled by photoinitiated shape programming. (Scale bar, 1 cm.) (*H*) Photographs of a multifunctional architecture. LM–LCE composites function as a conductive wire to run current through an LED, as a transducer to sense touch, and as a Joule-heated actuator to lift a weight. An LED turns on when the sensing composite responds to touch, and internal Joule-heated actuation is activated. An example of the process is shown in Movie S1. (Scale bar, 1 cm.)

stimulation (Fig. 1*G*). Critically, the LCE retains the ability to actively shape morph even for cases when up to 50 vol % (83 wt %) of the composite is filled with the mechanically passive LM droplets.

Immediately after synthesis, the composites are inherently electrically insulating due to the native oxide shell that forms around the LM microparticles, which contributes to stabilizing the LM microparticle dispersion (17). In this state, the composites exhibit a high thermal conductivity that improves heat distribution and response to thermal stimulation. Electrical conductivity can be induced by mechanical sintering (18), which irreversibly forms percolating LM pathways. Electrical conductivity in the composite can autonomously reconfigure when conductive traces are mechanically damaged (Fig. 1*E*). More generally, the composite's electrical conductivity enables the creation of internally Joule-heated actuators, transducers for touch sensing, and circuit wiring for surface-mounted electronic components (Fig. 1*H*). Joule-heated linear actuation of LM–LCEs can be excited at rates faster than 2 Hz and cycled to 50% reversible strain 15,000 times at 0.007 Hz (and 2.5% reversible strain >100,000 times at 1 Hz while still retaining >90% of its original shape change). Together, these properties enable the composite to display a rich diversity of functionalities that allows it to simultaneously exhibit sensing and dynamic responses (e.g., Fig. 1*H*).

Results and Discussion

LCEs were synthesized from a simple, one-pot methodology using commercially available precursors (*SI Appendix*, Fig. S1) (19). LM microparticles were introduced by shear mixing with an overhead mixer before curing the elastomer to form droplets of ~200 to 500 μm in size (Fig. 1*D*). The stress–strain characteristics of all composites measured were comparable to unfilled LCEs, showing 1) a linear response for small strains (*SI Appendix*, Fig. S2); 2) semisoft elasticity due to reorientation of the liquid crystal director as strain increases; and 3) an elastic regime before breaking. Composites across the range of LM loading were deformable with average maximum extensions >150% (Fig. 2*B*). Average tensile moduli ranged between 0.2 and 1.2 MPa for all loadings, characteristic of the compliance of the LCE and LM-LCEs (Fig. 2*C*). Both the unfilled LCE and 50 vol % LM–LCE had similar storage moduli across the temperature range measured by dynamic mechanical analysis (DMA, Fig. 2*D*). Generally, the mechanical properties of the LCE matrix were not drastically influenced by the presence of LM microparticles.

To maximize composite functionality, the LM microparticles should not inhibit shape-changing characteristics. With DMA, we find that the nematic-to-isotropic transition temperature is not influenced by LM inclusions, occurring at 65.5 ± 3.2 °C for the unfilled LCE and 64.7 ± 2.7 °C for the 50 vol % LM–LCE (Fig. 2*D*) and corresponding with a local minimum in the storage modulus. The 50 vol % LM-LCE composite could reversibly extend to and retract from 1.62 ± 0.10 times its original length, retaining >90% of actuation capabilities relative to an unfilled LCE at the same stress (1.74 ± 0.01 times its original length, Fig. 2*E*). As the applied stress increases, the reversible change in length increases (*SI Appendix*, Fig. S3), a property typical for LCE shape change (20). That the LM microparticles are functionally passive with respect to mechanical properties as well as actuation highlights a unique aspect of the composite we present here: Since the LM is deformable, the LCE matrix can deform along with the LM and retain intrinsic shape-changing capabilities. The rule of mixtures predicts a weighted average for materials properties in a composite, and we might have expected a drastic reduction in actuation capabilities at 50 vol % LM. Moreover, decreased actuation has been observed in rigid particle–LCE composites (11, 15). However, the deformable LM microparticles permit macroscopic shape change.

Having established that the compliance and shape-changing functionalities of the LCE matrix were not disrupted by the presence of LM droplets, we next examined the functionalities borne of the LM microparticles, particularly the thermal and electrical transport properties. The thermal conductivity of the composite increased relative to the thermal conductivity of the unfilled LCE as LM microparticle loading increased, as measured by the transient hot-wire technique (*SI Appendix*, Figs. S4 and S5). The thermal conductivities of LM loadings of 0, 10, 20, 30, and 50 vol % were 0.24 ± 0.02, 0.32 ± 0.04, 0.45 ± 0.02, 0.62 ± 0.09, and 1.70 ± 0.16 W $m^{-1}\cdot K^{-1}$, respectively (Fig. 2*F*). As with other LM-embedded elastomers, the thermal conductivity increased along the loading direction as the LM microparticles elongated (Fig. 1*D*) (21). LM–LCEs hold about 50–60% strain in a stress-free state due to reorientation of the liquid crystal director after being stretched. The thermal conductivity along the direction of strain increased for the unfilled LCE due to the change in liquid crystalline ordering from a polydomain to a monodomain (22). The average thermal conductivity of the unfilled LCE increased to 0.48 ± 0.02 W $m^{-1}\cdot K^{-1}$ (Fig. 2*G*) along the direction of strain and was as high as 2.48 ± 0.46 W $m^{-1}\cdot K^{-1}$ for 50 vol % LM–LCE (Fig. 2*H*). For

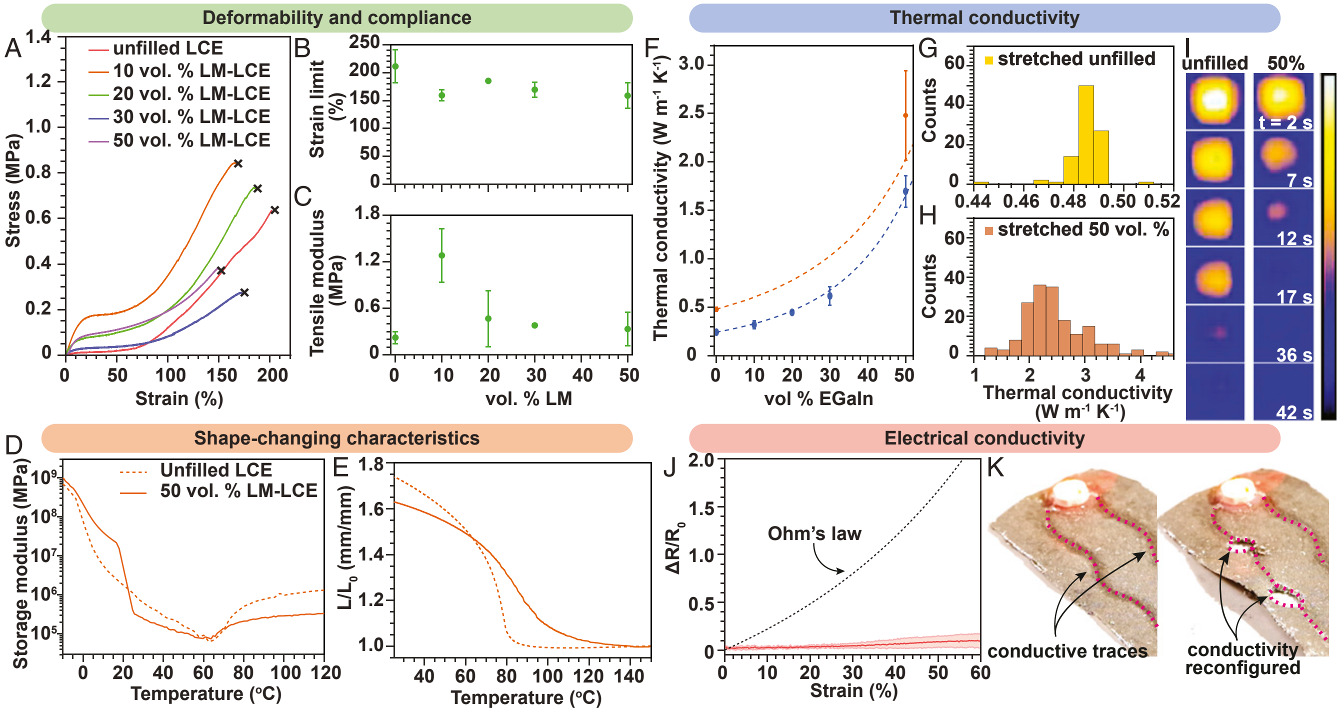

Fig. 2. Material properties of LM–LCE composites. (*A*) Representative stress versus strain for LCEs and LM–LCE composites; (*B*) strain limit at break and (*C*) tensile modulus. Error bars represent SD for ≥ 3 measurements. (*D*) Representative storage modulus versus temperature for filled and unfilled materials. (*E*) Representative normalized length change versus temperature during cooling for filled and unfilled materials with a 20-kPa applied load. (*F*) Thermal conductivity versus volume fraction for unstretched materials for $n \geq 300$ measurements with at least 3 samples tested for each volume fraction (blue circles), and for stretched unfilled LCE and 50 vol % LM–LCE, deformed to about 60% elongation ($n \geq 100$, orange circles). Error bars represent SDs. The dashed traces represent the theoretical predictions using the Bruggeman effective medium theory formulation (blue) and a modified Bruggeman effective medium formulation for elongated inclusions (orange) (21, 23). (*G* and *H*) Histograms of thermal conductivity along the direction of strain (at 60% strain) for a 50 vol % LM–LCE composite and an unfilled LCE; (*I*) IR heat map showing heat dissipation of a 50 vol % LM–LCE composite and an unfilled LCE after initial heating. The temperature scale ranges from 20 °C (blue) to 120 °C (orange). (*J*) Normalized change in electrical resistance, *R*, versus strain of a conductive LM–LCE strip with the red line representing the average and the shaded region representing the SD for 3 samples tested 3 times each ($n = 9$) with a comparison to predictions from Ohm's law (dashed curve). (*K*) Photographs of autonomous self-reconfiguring electrical conductivity upon puncturing through the traces.

comparison, the average thermal conductivities perpendicular to the direction of strain were 0.25 ± 0.003 W m^{-1}·K^{-1} for the unfilled LCE and 1.86 ± 0.10 W m^{-1}·K^{-1} for the 50 vol % LM–LCE. The measured thermal conductivities are in good agreement with predictions from the Bruggeman formulation of effective medium theory for a uniform dispersion of spherical conductive particles in a thermally insulating matrix for the unstrained case. The experimental results are also in good agreement with a modified Bruggeman formulation for elongated conductive particles for the strained case (21, 23). Enhancements of thermal conductivity by a factor of 2 in the unfilled LCE arises from strain-induced molecular reorientation and is comparable to prior studies of liquid crystal polymers at similar strain (22, 24). To visualize the increase in thermal conductivity, 50 vol % LM–LCE and unfilled LCE samples were heated and placed side by side on a heat sink, and heat dissipation was observed by a thermal camera. The 50 vol % LM–LCE cooled quicker relative to the unfilled LCE (Fig. 2*I*). Improvements in thermal conductivity and heat dissipation are important for Joule-heated actuation but also wearable electronics and soft machines that interface conductors and insulators with electronic devices, which may overheat with use.

Electrical conductivity can be induced through a process of mechanically controlled LM sintering (18). An applied pressure ruptures the LM droplets, which then coalesce to form electrically conductive pathways. Depending on where pressure is applied, conductivity can be limited to selective circuit traces or active throughout the entire sample. Electrical conductivities for 50 vol % LM–LCEs where the entire sample was mechanically sintered were 1 × 10^4 to 2 × 10^4 S/m. The normalized change in resistance was monitored as a function of strain to evaluate electromechanical coupling for the 50 vol % LM–LCE (Fig. 2*J*). Consistent with previously reported conductive LM-embedded elastomers (25, 26), there is negligible electromechanical coupling up to 60% strain when compared to the change in normalized resistance expected according to Ohm's law. Conductive traces were observed to be self-healing through mechanisms previously reported for LM–silicone composites (25) in which mechanical damage activated the formation of new conductive traces (Fig. 2*K*). Conductivity was stable when 1 V was applied for >65,000 s (18 h), which is important for applications that require long-term Joule heating (*SI Appendix*, Fig. S6).

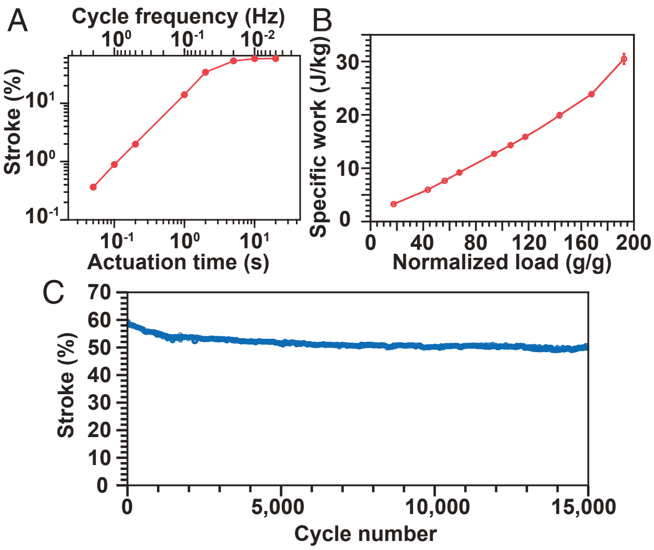

Fig. 3. Joule-heated actuation properties of LM–LCE composites. (*A*) Normalized stroke as a function of cycling frequency and actuation time (i.e., active duty cycle), for the 50 vol % LM–LCE to lift the hanging weight. SDs for $n \geq 4$ actuation cycles were less than 8% of the measured values. (*B*) Specific work as a function of normalized load for a 50 vol % LM–LCE. Error bars represent SDs for ≥3 actuation cycles. (*C*) Normalized stroke over 15,000 cycles for a 50 vol % LM–LCE actuating with a 14-kPa hanging wait at a frequency of 0.007 Hz.

LM–LCE composites that are electrically conductive can function as electrically responsive actuators that activate through Joule heating. Macroscopic deformation was observed as a weight was lifted, and multiple actuation cycles of 8 s on and 35 s off were tracked, showing repeatability in both the actuator displacement and power consumption (*SI Appendix*, Fig. S7). We measured how quickly the composite could actuate by tracking the normalized stroke as a function of cycle frequency (Fig. 3*A*). The actuation time, i.e., the active time period of the duty cycle, was set to 1/9th that of the cooling time. Cycling frequencies as high as 10 Hz with actuation times as low as 10 ms were perceptible (Movie S2 and *SI Appendix*, Fig. S8), although a normalized stroke could not confidently be evaluated (*SI Appendix*, Fig. S8). The normalized stroke increased up to 0.02 Hz, where it remained nominally constant at 0.5 (i.e., 50% output strain at about 10 to 15 kPa, Movie S2). Actuation times on the order of hundreds of milliseconds for actively heated LCEs have been previously reported, and actuation strains at a given frequency for the soft composite are consistent with previously reported LCEs that use rigid fillers (9, 15). Cycling frequency in Joule-heated composites is limited by heat dissipation to the ambient environment. Thermal diffusion in the composite has a timescale approximated by the sum of internal conduction and external convection time constants, $\tau \sim (L^2C/k + LC/h)$, where L is the thickness, k is the thermal conductivity, h is the convective heat transfer coefficient of the surrounding medium, and C is the volumetric heat capacity. For h = 10 W m^{-2}·K^{-1} (typical for free convection of air) and L = 0.5 mm, τ for the 50 vol % LM–LCE composite is convection limited to 80 through 90 s, similar to the cooldown time at 0.01-Hz cycling. For $h \to \infty$, the inclusion of LM microparticles decreases the conduction-limited τ by a factor of about 4 to 5 from 1,200 to 1,400 ms for unfilled LCEs to 200 through 300 ms, a tangible advantage when the composite is surrounded by a liquid (e.g., water, Movie S3).

The maximum specific work density of the LM–LCE composite was 30.5 J/kg, comparable to the maximum work density of mammalian skeletal muscle (27), and corresponding to a normalized dead load that was 193× the mass of the sample before mechanical failure during the 4th actuation cycle (Fig. 3*B*). For comparison purposes, the intrinsic work density of the LCE matrix when normalized with respect to the mass of only the stimuli-responsive matrix material (i.e., 17% of the composite mass) is estimated to be as high as 179 J/kg. This calculation assumes that the mechanically inactive LM particles do not contribute significantly to actuation (e.g., due to interfacial effects). Such an assumption is consistent with mechanical analyses that show that the LM microparticles do not influence mechanical properties of the composite. Specific work densities for unfilled LCEs and LCE composites reported in the literature are between 2 and 300 J/kg, with the highest values obtained for LCEs that are heated ambiently (27–29). To test cycling durability, a 50 vol % LM–LCE was subjected to 15,000 cycles at 0.007 Hz (Fig. 3*C*). The composite reversibly actuated to 50% strain over 15,000 cycles. Similar durability was observed when the composite was actuated >100,000 times at 1 Hz to a strain of 2.5% (*SI Appendix*, Fig. S9). Since Joule heating is uniform throughout the composite, shape change is resilient to damage (Fig. 4*A*). The composite can continue to lift a load by internal Joule heating after sustaining significant damage. Furthermore, the composite operates normally in cold environments and when struck with a hammer (Movie S4). A soft crawler comprising a bilayer structure of a silicone elastomer atop a stretched LM–LCE, represents an additional useful demonstration of actuation (Fig. 4*B* and Movie S5). The composite can also sense and respond to damage since mechanical forces activate conducting pathways. Conductive traces to power a light-emitting diode (LED) were induced in a 50 vol % LM–LCE composite.

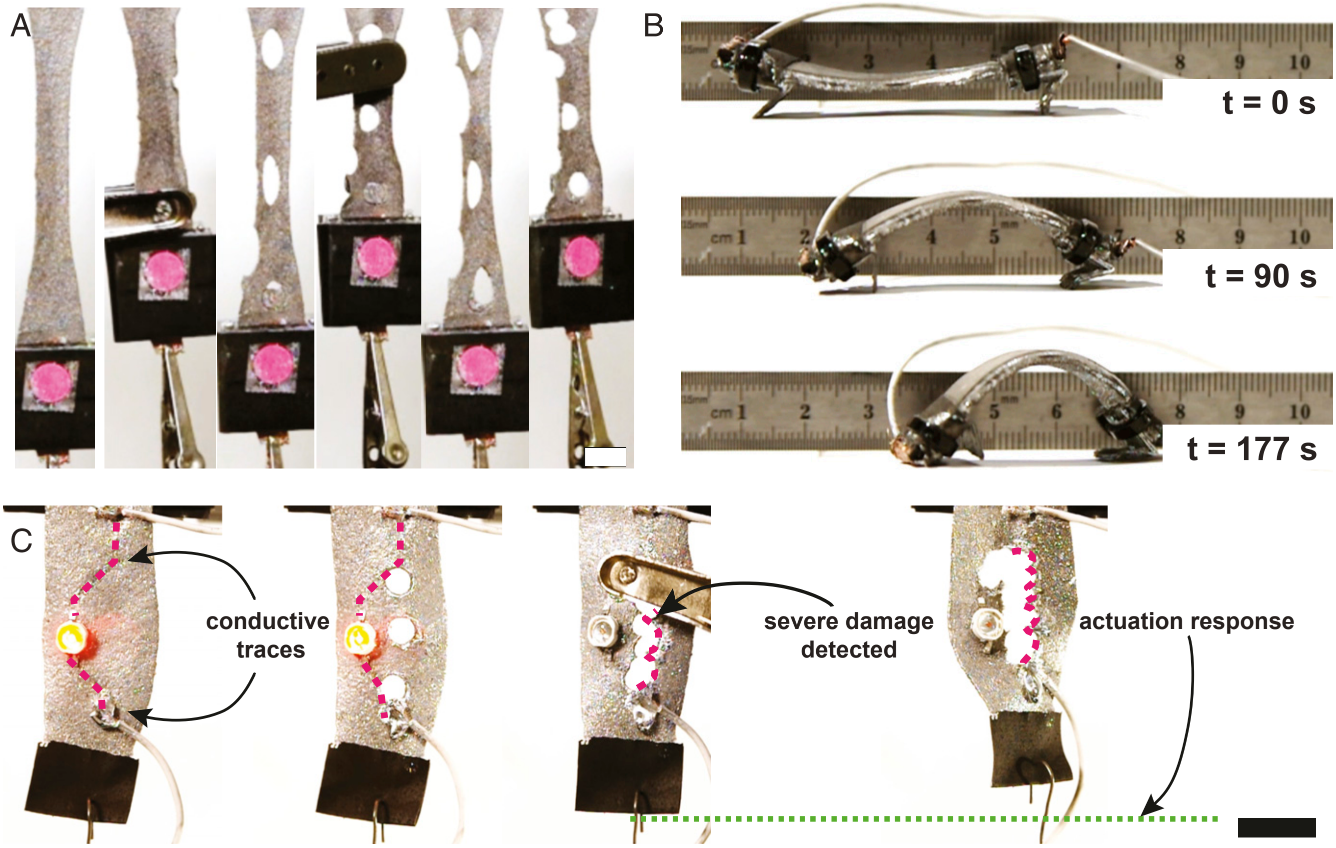

Fig. 4. (*A*) Sequence of damage resilience of a Joule-heated 50 vol % LM-LCE lifting a hanging weight. The sample continues to lift the weight after being punctured. (Scale bar, 10 mm.) (*B*) Sequence of soft crawler composed of a 50 vol. % LM-LCE. A ruler is used for scale. (*C*) Damage detection and response of an LM–LCE composite. In the first panel, a conductive trace powers an LED. As the sample is damage (second panel), the LED remains on. After severe damage, Joule heating lifts the weight hanging from the composite (third and fourth panels). (Scale bar, 20 mm.)

Mechanical damage can cause an electrical short around the LED, and the electrical current is rerouted through the composite. Referring to Fig. 4*C*, the rerouted current initiates Joule-heated actuation of the LCE and causes the composite to contract. We note that the mechanical damage must be substantial enough to rupture and coalesce LM microparticles and reroute percolation pathways. The composite can be stretched, deformed, and prodded without inadvertently activating new traces (Movie S4), which was also true for previously reported silicone-based composites (25). Together, this autonomous damage response, along with the soft crawler and capacitively controlled actuator shown in Fig. 1*H*, demonstrate the versatility in material functionalities that this composite offers, with the composite capable of functioning as a transducer, conductor, and actuator.

Thus far, the LCEs and LM–LCE composites discussed here were cured without a preferential orientation of the nematic director; that is, the microstructure is polydomain, with liquid crystal moieties that are locally oriented but macroscopically isotropic. However, the LCEs used in this study can also be irreversibly programmed using a photoinitiated postcuring process to lock in the molecular orientation of the LCE after mechanical deformation (19). The appeal of photoinitiated programmability includes actuation in the absence of a bias stress and controlled spatially patterned shape change that could see use in deployable and morphing structures. At zero applied stress, a linearly programmed 50 vol % composite reversibly elongated to 1.53 ± 0.09× its contracted length, compared to 1.61 ± 0.06 for a linearly programmed unfilled LCE (*SI Appendix*, Fig. S10). Blocking stress at failure for a linearly programmed 50 vol % LM–LCEs was 119 ± 36 kPa, on the same order of magnitude as state-of-the-art multifunctional dielectric actuators (300 kPa) and natural muscle (100–350 kPa), (*SI Appendix*, Fig. S11) (27, 30). Complex shape changes are possible with simple modifications to the strain field during programming, and the use of an opaque stencil mask during UV exposure. Fig. 1*G* illustrates an example of complex zero-stress shape change. The composite undergoes shape change from multiple half-cones to a flat geometry, as previously predicted (31). Additional complex shape-changing structures are shown in Movie S6. Because the composites are electrically conductive, such shape change can be induced by internal Joule heating, as shown for a radially programmed structure in Movie S6. Joule heating can also be activated asymmetrically, enabling bistable—and feasibly, multistable—programmable structures. An example of asymmetric Joule heating, where opposite sides of a linearly programmed composite are activated sequentially, is shown in Movie S7 and captured by thermal imaging (*SI Appendix*, Fig. S12). The structure contracts on the side that is activated, and the monolithic composite slides as each side contracts. The programmability of the LCE matrix is not detrimentally disrupted by the presence of LM and thus is a beneficial additional functionality of the composite.

A unique aspect of this work relative to previously reported LCE composites is that the filler material is deformable rather than rigid. For LCE composites with rigid fillers, electrical and thermal conductivity can be improved relative to the unfilled LCE but the shape-memory actuation capabilities are significantly impaired (15). The LCE composite that we introduce here has high electrical and thermal conductivity while retaining its natural actuation capabilities. The deformability of the LM microparticles appears to be integral to preserving actuation capabilities at high filler content. When solid gallium microparticles are used, the composite

[Ga–LCE, designated (s) or (l) for solid or liquid gallium microparticles] was rigid with a tensile modulus >10× larger than the unfilled LCE and either 50 vol % LM- or Ga-LCE (s) (Fig. 5 *A* and *B*). The Ga–LCE (s) composites began to visually tear at less than 10% strain. Gallium microparticles can be melted at a temperature less than the LCE nematic-to-isotropic transition (T_{ni}, *SI Appendix*, Fig. S13). Upon melting the gallium microparticles, the Ga–LCE (l) could extend to >50% strain (Fig. 5*C*). With further heating to above T_{ni}, the Ga–LCE (l) reversibly contracted since the inclusions were in the deformable, liquid state (Fig. 5*D* and Movie S8). An aspect of utilizing Ga–LCE vs. LM–LCE is the ability to achieve zero-stress actuation without photoinitiated cross-linking. We first uniaxially extended a Ga–LCE (l) composite and then cooled the composite to solidify the Ga inclusions. By selectively Joule heating certain regions of the composite, rigid and deformable domains can coexist in a monolithic composite. The deformable regions of the Ga–LCE composite can be selectively heated above T_{ni} by Joule heating. Since the rigid regions were constrained while the deformable regions attempted to contract, curvature and buckling was observed (Fig. 5 *E*–*H* and Movie S8). Ga–LCE (l) and (s) composites reveal the mechanism by which high filler loading LCEs remain mechanically functional while also introducing an additional route to unique and arbitrary shape morphing of our LCE composites.

Conclusion

In closing, emerging applications in soft robotics, wearable computing, and physical human–machine interaction require materials that match the rich versatility and multifunctionality of soft biological tissue. LCEs are promising due to their compliance and shape-morphing properties but have been limited by their inadequate intrinsic thermal or electrical conductivity as well as mechanical incompatibility with traditional rigid fillers. Here, we show that embedding LCEs with LM microparticles allows for enhancements in thermal and electrical properties without significantly altering compliance, strain limit, or shape-memory response. The significance of our findings is 2-fold: 1) previous composites using LCEs could not actuate by Joule heating with significant volume fraction of rigid fillers, therefore limiting electrical and thermal conductivity. In contrast, high volume fraction fillers are not detrimental to actuation capabilities for the case of deformable LM particles. 2) Compared to previous efforts with LM-embedded elastomers, the composite presented here represents a shift to multifunctional materials where the matrix has an active role in functionality (e.g., shape morphing). The unique combination of material properties and dynamic functionalities in our LM–LCE composite leads to emergent behaviors such as coupled sensing and actuation that could have transformative impact on the use of LCEs in soft-matter engineering.

Materials and Methods

Detailed procedures are provided in *SI Appendix*.

LM–LCE Composite Synthesis. LCEs were synthesized following a modified version of a previously reported procedure (19). EGaIn was made by mixing 75 wt % Ga (RotoMetals, 99.99%) with 25 wt % In (RotoMetals, 99.99%) at 100 °C until In was completely dissolved. EGaIn was added to the uncured LCE mixture before adding catalyst by shear mixing with a Scilogex OS20-S overhead stirrer with a 316L stainless-steel cross-stirrer attachment at 500 rpm for 30 s. After adding catalyst, the composite cured for >5 h before placing the composite in an 85 °C vacuum oven for >8 h.

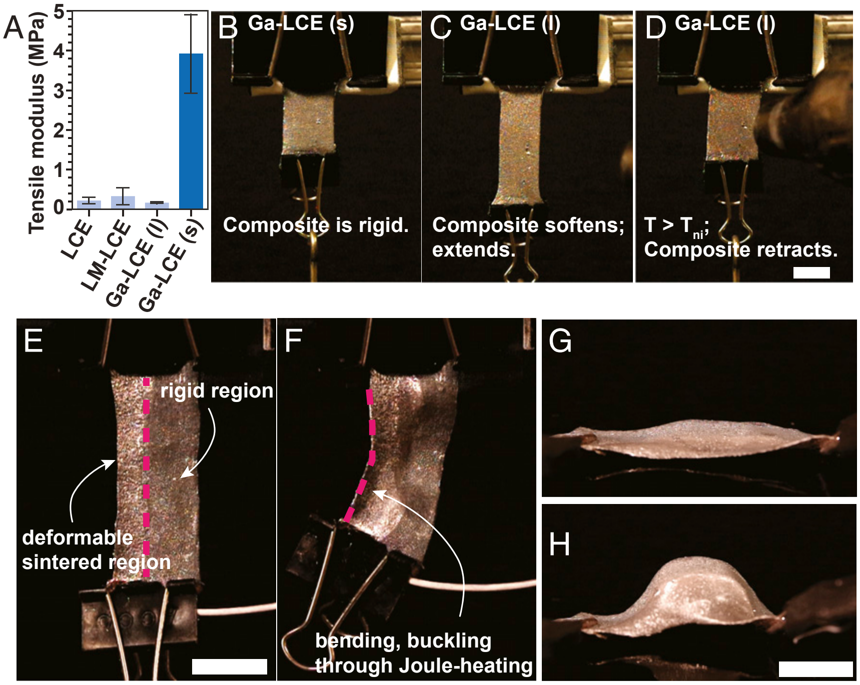

Fig. 5. Influence of inclusion deformability on composite properties. (*A*) Tensile moduli for unfilled LCE, 50 vol % LM–LCE, 50 vol % Ga–LCE (l), and 50 vol % Ga–LCE (s) where the (l) and (s) designations refer to the physical state of the gallium microparticles (liquid or solid). Measurements were made at room temperature. Error bars represent SDs for ≥3 measurements. (*B*) Photograph of Ga–LCE (s) with a hanging weight. The rigid inclusions do not permit extension. (*C*) Photograph of Ga–LCE (l) with a hanging weight. A heat gun is visible, providing heat to melt the gallium inclusions and permitting the composite to extend. (*D*) Photograph of Ga–LCE (l) after heating above the nematic-to-isotropic transition temperature (T_{ni}) of the LCE. The composite is able to retract to its original position. (Scale bar, 20 mm.) (*E*) Photograph of a hanging Ga–LCE composite with specific regions selectively heated to form rigid (solid Ga inclusions) and deformable (liquid Ga inclusions) domains. The deformable domain is mechanically sintered to induce electrical conductivity. (Scale bar, 20 mm.) (*F*) Photograph of a hanging Ga–LCE bending and buckling during Joule heating due to the rigid domain resisting contraction while the deformable domain contracts. (*G*) Photograph of a flat Ga–LCE with specific regions selectively heated to form rigid and deformable domains. (*H*) Photograph of a Ga–LCE bending and buckling during zero-stress actuation induced by Joule heating. (Scale bar, 20 mm.)

Thermo- and Electromechanical Characterizations. Stress–strain characteristics were evaluated by mechanical testing using an Instron 5969. For electromechanical characterization, a USB data acquisition module (USB-6002, NI) was used to collect analog data from the Instron 5969 while also recording resistance data from a voltage divider. The data were collected with MATLAB, 2018a (MathWorks, Inc.). DMA and thermal actuation characterizations were performed using a TA Instruments RSA-G2. At least 3 samples were tested for all mechanical characterizations.

Transient Hot-Wire Thermal Conductivity. The transient hot-wire method was used to determine the thermal conductivity as described in previous reports (21). The change in temperature vs. time was measured using a Keithley 2700 digital multimeter and a Keithley 6221 dc/ac current source in a 4-point measurement configuration with MATLAB 2014a.

Actuation Characterization. A Korad KA3010d precision variable adjustable power supply was used as the power source. To reduce contact resistance, a thin layer of EGaIn was spray-coated atop the composite where contacts were clamped in place. Position and actuation were tracked by either digital video or timelapse photography using MATLAB, 2018a. For actuation time/cycle frequency characterizations, the power supply was interfaced with a microprocessor (Arduino Uno), and power was cycled using a MOSFET.

Multifunctional Demonstrations. For the multifunctional composite demonstrated in Fig. 1*H*, the composite was connected to an Arduino Uno and a pin's capacitance was monitored using the capacitive sensing library. Another sample of the composite was linked to a high-power LED, and the microprocessor was used to change states of the LED when the capacitance achieved a defined threshold. Simultaneously, a high-voltage relay signaled the power supply to activate Joule heating an additional sample of the composite, lifting the hanging load.

For the soft crawler shown in Fig. 4*B*, a thin layer of epoxy and Sylgard 184 was secured atop a prestretched LM–LCE composite. Stainless-steel feet were used for asymmetric friction to drive the crawling robot forward.

For the damage-sensing composite shown in Fig. 4*C*, the composite was mechanically sintered to form conductive traces connecting a high-power LED. When the composite was initially damaged, there was no change in the state of the composite. When the damage was significant enough that it connected the conducting wires and electrically shorted the LED circuit, Joule heating was possible, and the hanging weight was lifted.

For preprogrammed samples as shown in Fig. 1*G*, the composites were programmed by stretching prescribed orientations by hand to 40 through 60% strain and masking with an opaque sheet of acrylic, if necessary. *SI Appendix*, Fig. S14 shows a schematic of the process to pattern programmed samples. Mechanical stretching has been shown to be effective in aligning liquid crystal domains in nominally thick samples (29). The sample was exposed to UV irradiation by a handheld UVL-56 UV lamp (365-nm wavelength) for >5 min on each side of the composite. Photographs and micrographs were processed using Adobe Lightroom for color correction with all adjustments applied equally across the entire image.

Gallium Microparticle LCE. A 50 vol % Ga–LCE composite was fabricated by melting gallium in a 100 °C oven and shear mixing to form Ga microparticles after allowing Ga to cool without resolidifying. For rigid composites, Ga particles were solidified after curing. For Ga–LCE (s) composites, Ga–LCE (l) samples were frozen after tensile testing, and elastic moduli were determined from the first strain cycle since visible tearing occurred on subsequent cycles. Joule-heated Ga–LCEs with selective regions of (s) and (l) Ga microparticles were first mechanically sintered in regions that were to remain (l). Then the entire composite was uniaxially stretched and frozen, followed by Joule heating of the sintered regions to re-form Ga–LCE (l) domains. Zero-stress actuation was induced by Joule heating as described previously in our methods.

ACKNOWLEDGMENTS. This material is based upon work supported by, or in part by, the US Army Research Laboratory and the US Army Research Office under Contract/Grant W911NF1810150 (Program Manager: Dr. Samuel C. Stanton).

1. T. J. White, D. J. Broer, Programmable and adaptive mechanics with liquid crystal polymer networks and elastomers. *Nat. Mater.* **14**, 1087–1098 (2015).
2. S. I. Rich, R. J. Wood, C. Majidi, Untethered soft robotics. *Nat. Electron.* **1**, 102–112 (2018).
3. C. Yang, Z. Suo, Hydrogel ionotronics. *Nat. Rev. Mater.* **3**, 125–142 (2018).
4. Y. Liu, M. Pharr, G. A. Salvatore, Lab-on-skin: A review of flexible and stretchable electronics for wearable health monitoring. *ACS Nano* **11**, 9614–9635 (2017).
5. M. Behl, M. Y. Razzaq, A. Lendlein, Multifunctional shape-memory polymers. *Adv. Mater.* **22**, 3388–3410 (2010).
6. S. M. Mirvakili, I. W. Hunter, Artificial muscles: Mechanisms, applications, and challenges. *Adv. Mater.* **30**, 1704407 (2018).
7. S.-J. Jeon, A. W. Hauser, R. C. Hayward, Shape-morphing materials from stimuli-responsive hydrogel hybrids. *Acc. Chem. Res.* **50**, 161–169 (2017).
8. H. Wermter, H. Finkelmann, Liquid crystalline elastomers as artificial muscles. *e-Polymers* **1**, 013 (2001).
9. M. Chambers, B. Zalar, M. Remškar, S. Žumer, H. Finkelmann, Actuation of liquid crystal elastomers reprocessed with carbon nanoparticles. *Appl. Phys. Lett.* **89**, 243116 (2006).
10. S. Courty, J. Mine, A. R. Tajbakhsh, E. M. Terentjev, Nematic elastomers with aligned carbon nanotubes: New electromechanical actuators. *Europhys. Lett. (EPL)* **64**, 654–660 (2003).
11. J. E. Marshall, Y. Ji, N. Torras, K. Zinoviev, E. M. Terentjev, Carbon-nanotube sensitized nematic elastomer composites for IR-visible photo-actuation. *Soft Matter* **8**, 1570–1574 (2012).
12. R. S. Kularatne, H. Kim, J. M. Boothby, T. H. Ware, Liquid crystal elastomer actuators: Synthesis, alignment, and applications. *J. Polym. Sci. Part B Polym. Phys.* **55**, 395–411 (2017).
13. M. Shahinpoor, "Electrically activated artificial muscles made with liquid crystal elastomers" in *Smart Structures and Materials 2000: Electroactive Polymer Actuators and Devices (EAPAD)* (International Society for Optics and Photonics, 2000), vol. 3987, pp. 187–193.
14. L. Yang, K. Setyowati, A. Li, S. Gong, J. Chen, Reversible infrared actuation of carbon nanotube–liquid crystalline elastomer nanocomposites. *Adv. Mater.* **20**, 2271–2275 (2008).
15. A. Agrawal *et al*., Electromechanically responsive liquid crystal elastomer nanocomposites for active cell culture. *ACS Macro Lett.* **5**, 1386–1390 (2016).
16. C. Wang *et al*., Soft ultrathin electronics innervated adaptive fully soft robots. *Adv. Mater.* **30**, e1706695 (2018).
17. M. D. Dickey, Stretchable and soft electronics using liquid metals. *Adv. Mater.* **29**, 1606425 (2017).
18. J. W. Boley, E. L. White, R. K. Kramer, Mechanically sintered gallium-indium nanoparticles. *Adv. Mater.* **27**, 2355–2360 (2015).
19. C. M. Yakacki *et al*., Tailorable and programmable liquid-crystalline elastomers using a two-stage thiol–acrylate reaction. *RSC Adv.* **5**, 18997–19001 (2015).
20. A. R. Tajbakhsh, E. M. Terentjev, Spontaneous thermal expansion of nematic elastomers. *Eur. Phys. J. E* **6**, 181–188 (2001).
21. M. D. Bartlett *et al*., High thermal conductivity in soft elastomers with elongated liquid metal inclusions. *Proc. Natl. Acad. Sci. U.S.A.* **114**, 2143–2148 (2017).
22. J. Shin *et al*., Thermally functional liquid crystal networks by magnetic field driven molecular orientation. *ACS Macro Lett.* **5**, 955–960 (2016).
23. P. N. Sen, C. Scala, M. H. Cohen, A self-similar model for sedimentary rocks with application to the dielectric constant of fused glass beads. *Geophysics* **46**, 781–795 (1981).
24. H. Chen *et al*., Thermal conductivity of polymer-based composites: Fundamentals and applications. *Prog. Polym. Sci.* **59**, 41–85 (2016).
25. E. J. Markvicka, M. D. Bartlett, X. Huang, C. Majidi, An autonomously electrically self-healing liquid metal-elastomer composite for robust soft-matter robotics and electronics. *Nat. Mater.* **17**, 618–624 (2018).
26. A. Fassler, C. Majidi, Liquid-phase metal inclusions for a conductive polymer composite. *Adv. Mater.* **27**, 1928–1932 (2015).
27. J. D. W. Madden *et al*., Artificial muscle technology: Physical principles and naval prospects. *IEEE J. Oceanic Eng.* **29**, 706–728 (2004).
28. T. H. Ware, M. E. McConney, J. J. Wie, V. P. Tondiglia, T. J. White, Actuating materials. Voxelated liquid crystal elastomers. *Science* **347**, 982–984 (2015).
29. M. O. Saed *et al*., Thiol-acrylate main-chain liquid-crystalline elastomers with tunable thermomechanical properties and actuation strain. *J. Polym. Sci. Part B Polym. Phys.* **55**, 157–168 (2017).
30. E. Acome *et al*., Hydraulically amplified self-healing electrostatic actuators with muscle-like performance. *Science* **359**, 61–65 (2018).
31. C. D. Modes, K. Bhattacharya, M. Warner, Gaussian curvature from flat elastica sheets. *Proc. R. Soc. London A Math. Phys. Eng. Sci.* **467**, 1121–1140 (2011).